INL/RPT-22-65701-Revision-0

Quarterly Management Document FY22, 1st Quarter, Multi-pass Hybrid Laser Arc Welding of Alloy 740H

January 2022

Thomas M Lillo, Todd Palmer

Changing the World's Energy Future

INL is a U.S. Department of Energy National Laboratory operated by Battelle Energy Alliance, LLC

INL/RPT-22-65701-Revision-0

Quarterly Management Document FY22, 1st Quarter, Multi-pass Hybrid Laser Arc Welding of Alloy 740H

Thomas M Lillo, Todd Palmer

January 2022

Idaho National Laboratory
Idaho Falls, Idaho 83415

http://www.inl.gov

Prepared for the
U.S. Department of Energy
Under DOE Idaho Operations Office
Contract DE-AC07-05ID14517

Quarterly Management Document – FY22, 1st Quarter, Multi-pass Hybrid Laser Arc Welding of Alloy 740H

Document # INL/RPT-22-65701

WBS Element	**Project Title**	**Contract Number**	**Contract Start**	**Contract End**
C.B.75.AA.01.01.01	Multi-pass Hybrid Laser Arc Welding of Alloy 740H	B100-19010	**10/01/19**	**09/30/2022**

Performer Name and Address	**Principal Investigator(s)**
Thomas Lillo Idaho National Laboratory P.O. Box 1625 Idaho Falls, ID 83415	Thomas Lillo

BUDGET AND COST REPORT

Prior Year Funds ($K)				**68.4**								
Total Current Year Commitment ($K)				**502.4**								
Projected Current Year Costs ($K)				**502.4**								
	O	**N**	**D**	**J**	**F**	**M**	**A**	**M**	**J**	**J**	**A**	**S**
Monthly Planned Costs	**12**	**12**	**12**	**26**	**56.2**	**71.2**	**47.0**	**64.1**	**54.1**	**53.0**	**47.0**	**47.0**
Actual Monthly Costs	**10.1**	**18.2**	**11.2**									
Monthly Variance	**1.9**	**-6.2**	**0.8**									
Total costs – planned	**12**	**24**	**36**	**62**	**118.2**	**189.4**	**236.4**	**300.5**	**354.6**	**407.6**	**454.6**	**501.6**
Total costs - actual	**10.1**	**28.3**	**39.5**									

MILESTONE REPORT

Milestone Designation	Milestone Description	Due Date	Revised Due Date	Completion Date
Task 1	Purchase and installation of Laser Wobble Head at INL and PSU	12/31/2019	3/15/2020	6/31/2020
Task 2	Single pass bead-on-plate welds with microstructure characterization – Effect of Laser Wobble Modes during HLAW	12/2020		12/30/2020
Task 3	Deep Penetration Land Welding Development and Optimization of Multi-pass HLA welds	7/2021	12/2021	01/10/2022
Task 4	Modeling of Deep Penetration Laser Welding	9/2021	4/2022	
Go/No Go Decision Pt #1	Performance of Deep Penetration Land Welds and HLAW filler weld material	7/2021	12/2021	01/10/2022
Go/No Go Decision Pt #2	Cycle time evaluation for thick land/HLAW thick (~1.25”) welds and their performance	12/2021	03/2022	
Task 5	Complete 3” thick weld (thick land laser weld + HLAW groove filling)	6/2022		
Task 6	Characterization – Microstructure & Mechanical properties of 3” thick weld	9/30/2022		

TECHNICAL HIGHLIGHTS

Task 1, Purchase and installation of Laser Wobble Head at INL and PSU

Completed.

Task 2, Single pass bead-on-plate welds with microstructure characterization – Effect of Laser Wobble Modes during HLAW

Completed.

Task 3, Deep Penetration Land Welding Development and Optimization of Multi-pass HLA Welds

Deep Penetration Laser Welding Progress:

Laser beam wobble welding which combines different oscillating trajectories of the laser beam along with translation motion has demonstrated potential of eliminating common welding defects like porosity, surface roughness and solidification cracks. Laser keyhole mode wobble welding of IN740H were conducted using several wobble amplitude and frequencies to study feasibility of crack free welding.

Solidification cracks

Cracks were observed in the fusion zone of the laser welds without wobble (Figure 1a). These cracks followed the grain boundary as shown from the inverse pole figure map (Figure 1b) and were identified as solidification cracks. When welded using a circular laser wobble with an amplitude of 1.6 mm and frequencies 150-475 Hz (Fig. 1c, 1e, and 1g), no cracks were observed. All the welds were characterized using CT scans and EBSD to identify and measure the location of the cracks within in the weld.

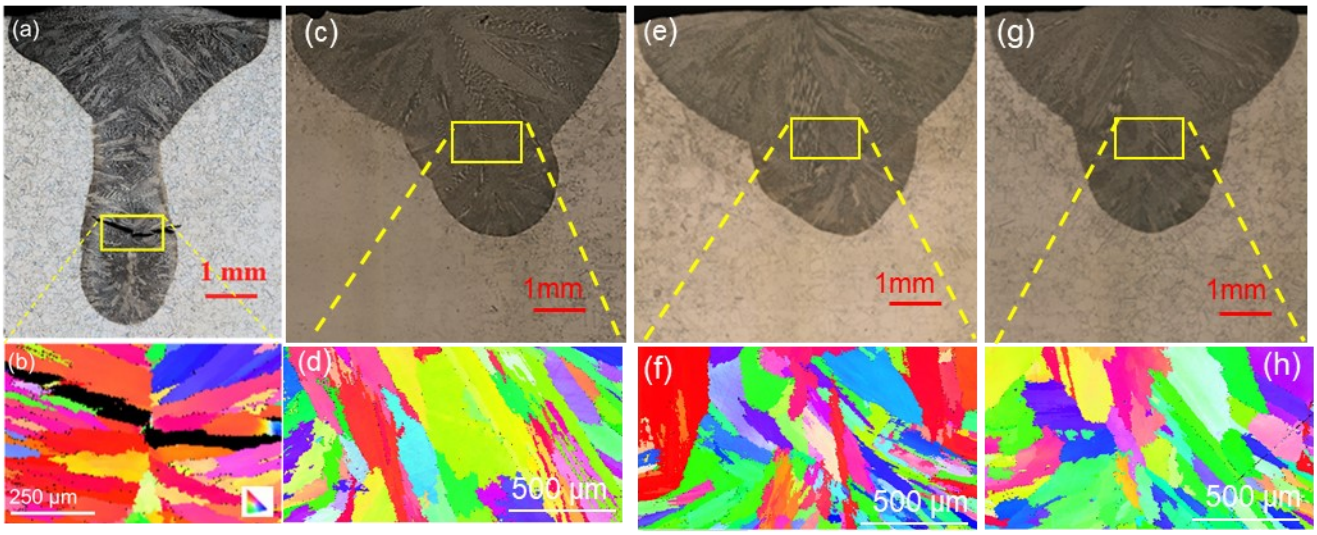

Figure 1. (a) Crack in fusion zone of laser weld without wobble for 5 kW, 12.7 mm/s. Wobble laser welds for 5kW,12.7 mm/s with 1.6 mm amplitude and frequencies of (c) 150Hz, (e) 300 Hz and (g) 475 Hz showed no cracks. Corresponding IPF maps of the weld are shown in (b), (d), (f) and (g).

Previous experiments showed that cracks occurred in all laser welds *without* laser wobble for powers ranging 5-10 kW and speed 12.7 mm/s -38.1 mm/s. Interestingly these cracks always occurred at intermediate depths in the keyhole finger but neither at the weld surface or weld root (Table 1). To understand the origin of solidification cracks in laser keyhole welding (without the wobble) and to identify their location, a heat transfer and fluid model of the process was developed and is described below in Task 4.

Multi-pass HLAW Weld Groove Filling Progress:

In the previous quarterly report, significant improvement to the hybrid laser arc weld (HLAW) quality was demonstrated in welds made using a circular laser wobble pattern, Figure 2a, and a "Figure 8" laser wobble pattern, Figure 2b, with only a number of small (< ≈1 mm) vertical cracks observed in the weld. Further improvements to the weld quality and the influence of the laser power on weld quality were investigated in an additional hybrid laser arc welding campaign during the 1st quarter of FY22. For this campaign, a laser wobble pattern in the form of a star was used, Figure 3, and HLAW groove-filling welds were made at laser powers of 2 kW and 3 kW using a travel speed of 508 mm/ minute (20 inches per minute) and constant weld wire feed speed of 7.5 m/minute. The goal of these welds was to reduce temperature gradients within the weld pool and mitigate cracking during solidification since modeling results for laser welding tend to indicate cracking becomes more likely as temperature gradients within the weld pool exceed a critical value (see discussion in Task 4 below). The laser wobble pattern and laser parameters, i.e., maximum wobble amplitude, used here tend to spread out the laser power over a greater area and, thereby, reduce temperature gradients.

Each HLA weld was cross sectioned and prepared for metallography. Figure 4 shows the microstructures found for each of the welds. The HLA weld made using 2 kW in Figure 4a contains a single, but significant, crack while the HLA weld made using a laser power of 3 kW does not exhibit any cracking or other significant defects. The results from this last hybrid welding campaign seem to imply a relationship between heat input (which is a function of travel speed, arc voltage and wire feed speed) and laser wobble amplitude. It appears the combination of the slower travel speed, the star laser wobble pattern and the higher laser power (3 kW) resulted in the best welds to date. Other combinations of parameters and wobble patterns may also result in similar high-quality welds, possibly even at higher travel speeds that might result in higher productivity gains. However, the laser power of the current INL laser system is nearly at its maximum and the laser wobble amplitude is also at its maximum. To achieve, high-quality hybrid welds similar to those in this latest campaign, it is thought that higher laser powers and/or laser wobble amplitude would be required for higher traverse velocities and, ultimately, modifications to the current system would be needed and are beyond the scope of this project. Additionally, as the traverse speed increases, the number of welding passes required to fill the weld groove increases (at a constant wire feed speed) which can actually *increase* the overall joining time since labor-intensive/time-consuming cleaning is required between subsequent weld passes, i.e., more passes require more total cleaning time which offsets the decreased weld time. Therefore, the current

hybrid parameters will be utilized within the limitation of the current hybrid laser arc welding equipment.

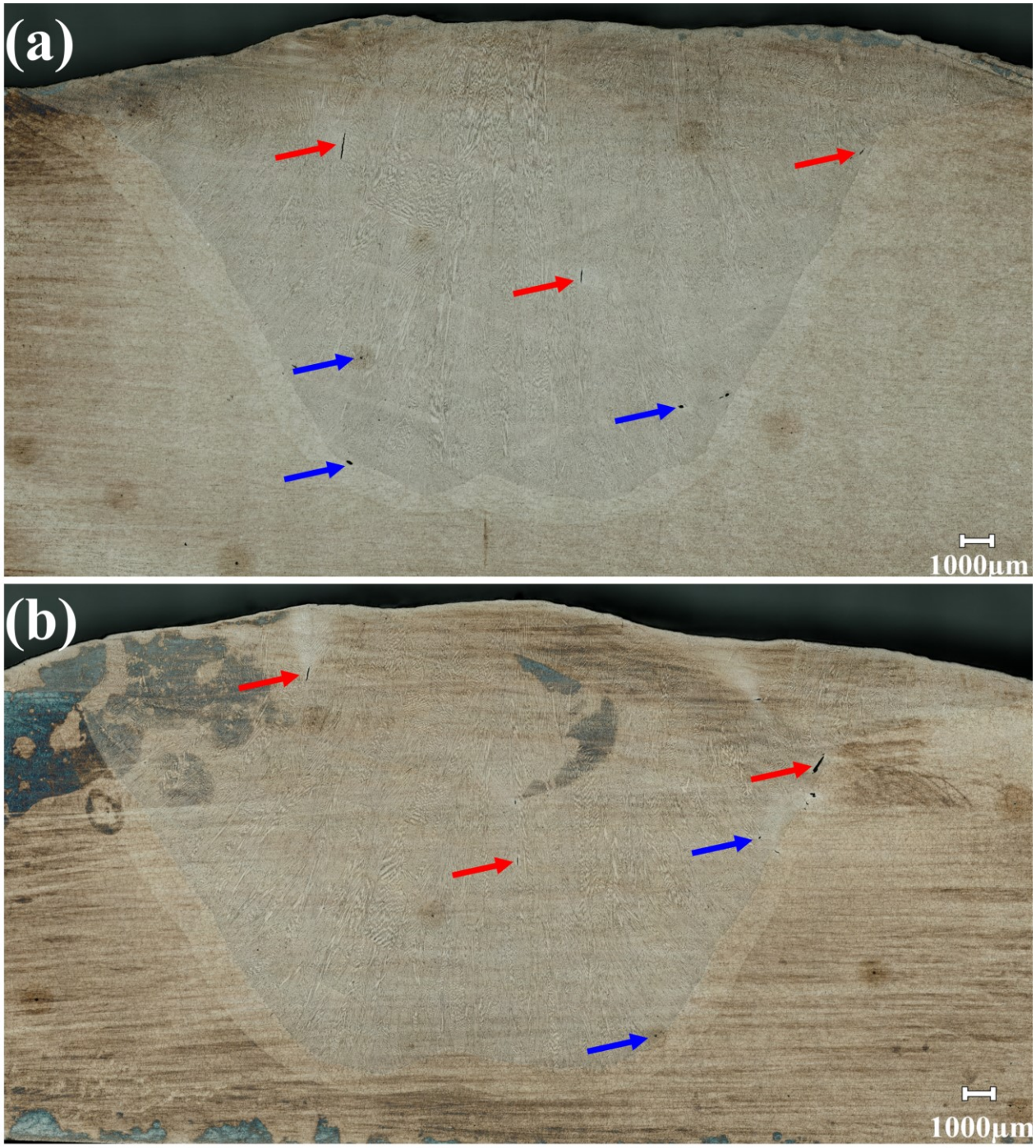

Figure 2. Weld microstructures for (a) Weld #4A, and (b) Weld #4B in Alloy 740H. The laser wobble pattern in (a) was circular while it was a "Figure 8" in (b). Laser power for both welds was 2 kW. Vertical cracks are indicated at the red arrows while more rounded defects are indicated by the blue arrows. Heavy etching to reveal the weld microstructure has resulted.

Conclusion: The results from this latest hybrid laser arc groove-filling campaign indicate an appropriate combination of arc welding and laser parameters has been found to produce high quality welds with minimal defects. Therefore, these welds are considered to be good candidates for the long term (~10,000 hr) creep tests to demonstrate creep behavior of these hybrid welds that is, as a minimum, equivalent to welds made by conventional GTAW methods in a previous project. Therefore, material from the hybrid welds shown in Figure 4a and Figure 4b has been sent to a commercial vendor to fabricate cross-weld creep specimens. These specimens will be creep tested using conditions expected to produce relatively short creep lifetimes, ~200-300 hrs, (see Table 2, below) as well as conditions (TBD) to result in creep lifetimes on the order of 10,000 hrs to validate these HLA welds. Both short-term and long-term creep tests are expected to be started during the 2nd quarter of FY22. Therefore, this task which is focused on the search for laser welding and HLA welding parameters is considered complete.

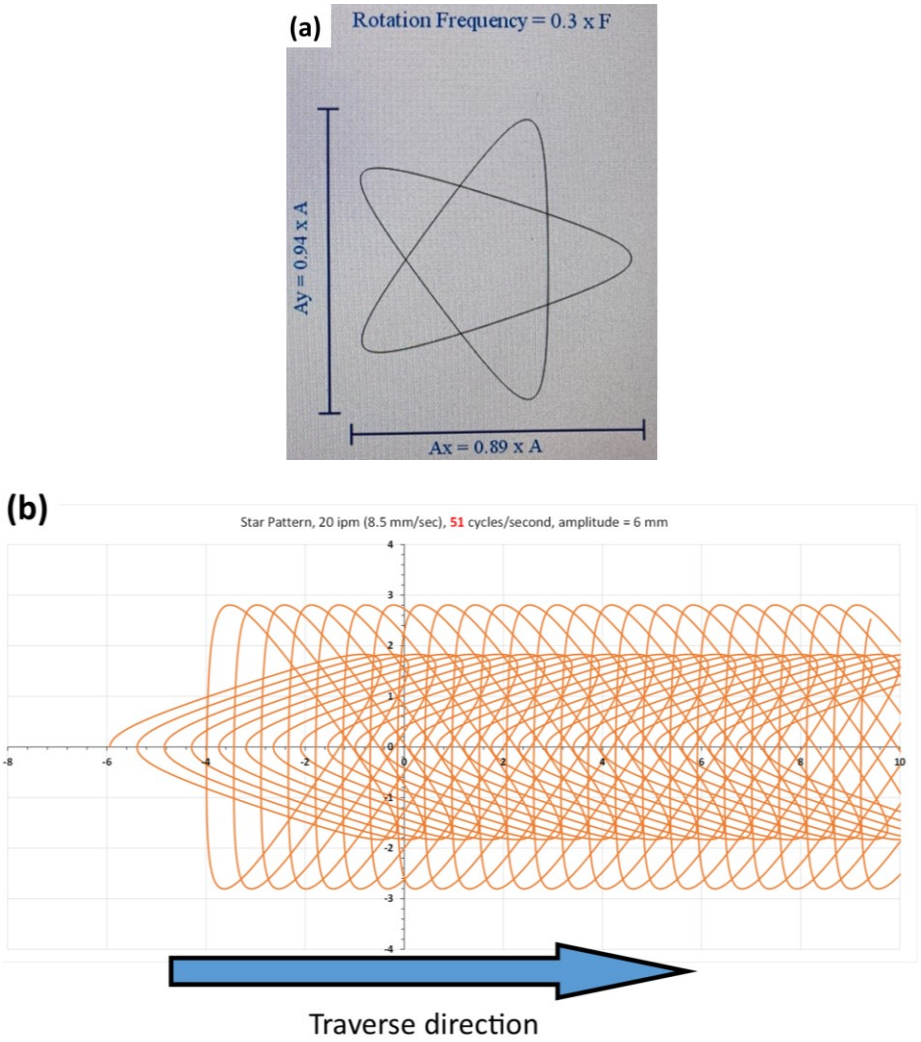

Figure 3. (a) Star-shaped laser wobble pattern and (b) path of the laser beam during welding at 508 mm/minute.

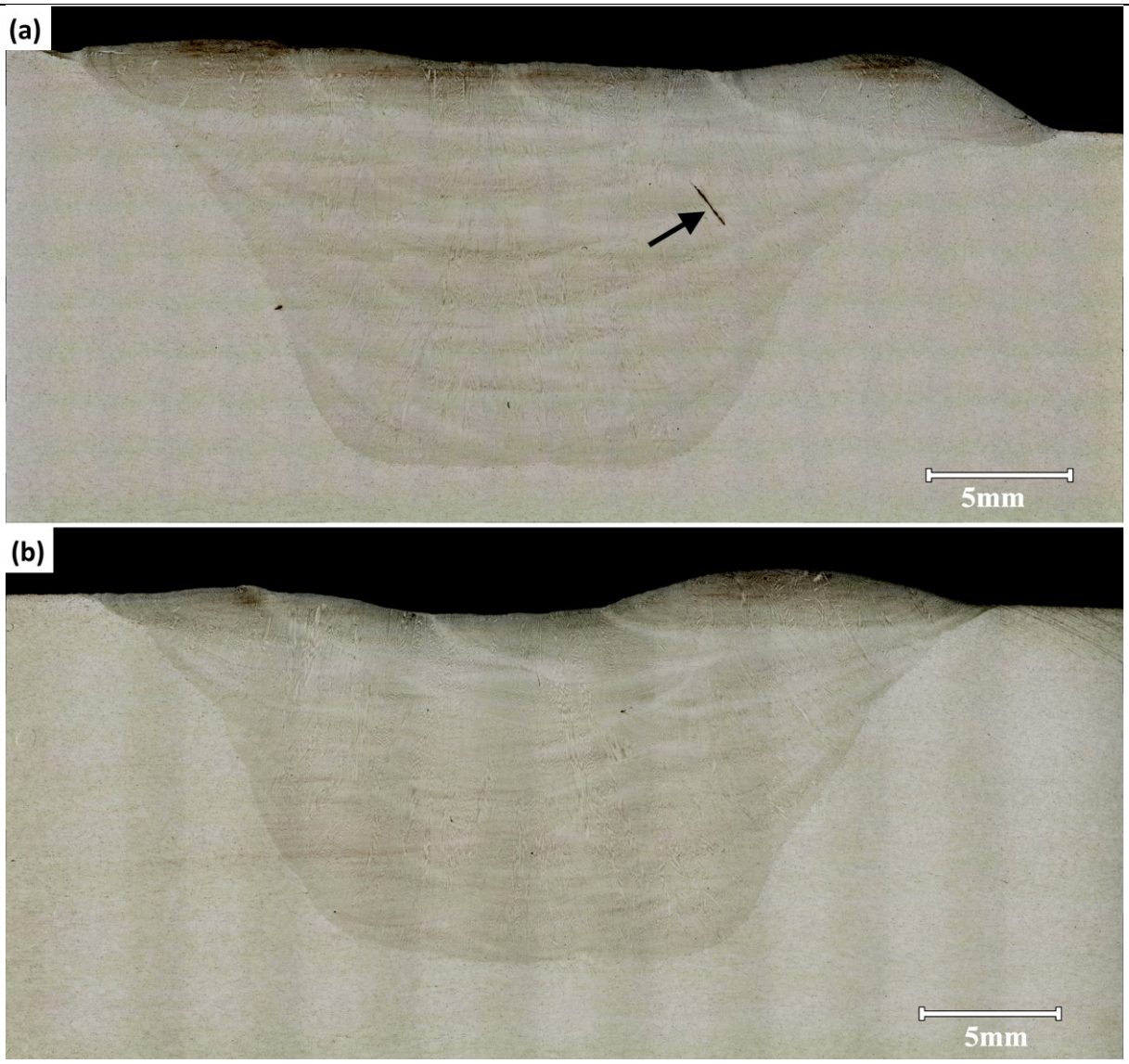

Figure 4. (a) Cross section of the hybrid weld using the star laser wobble pattern, travel speed of 508 mm/minute and laser power of 2 kW, and (b) cross section of the hybrid weld using the star laser wobble pattern, travel speed of 508 mm/minute and laser power of 3 kW. The arrow in (a) indicated a crack.

Task 4, Modeling of Deep Penetration Laser Welding

Laser keyhole modeling without the use of wobble was developed and validated for various welding conditions previously. A quantitative investigation of solidification cracking in deep penetration keyhole mode welding requires knowledge of the temperature field, solid fraction distribution, and the fusion zone geometry for various welding variables. A 3D isometric view of the molten pool using 5 kW and 12.7 mm/s welding speed is shown in Figure 5. Heat transfer by conduction and convection in three dimensions affects the shape and size of the fusion zone. The keyhole geometry is indicated by the red-colored region enclosed by the boiling point of the alloy which is 3063 K. The mushy zone is bound by the liquidus

temperature surface of 1669 K and the solidus temperature field of 1425 K. The weld pool and the mushy zone lengths decrease with increasing depth measured from the weld pool surface.

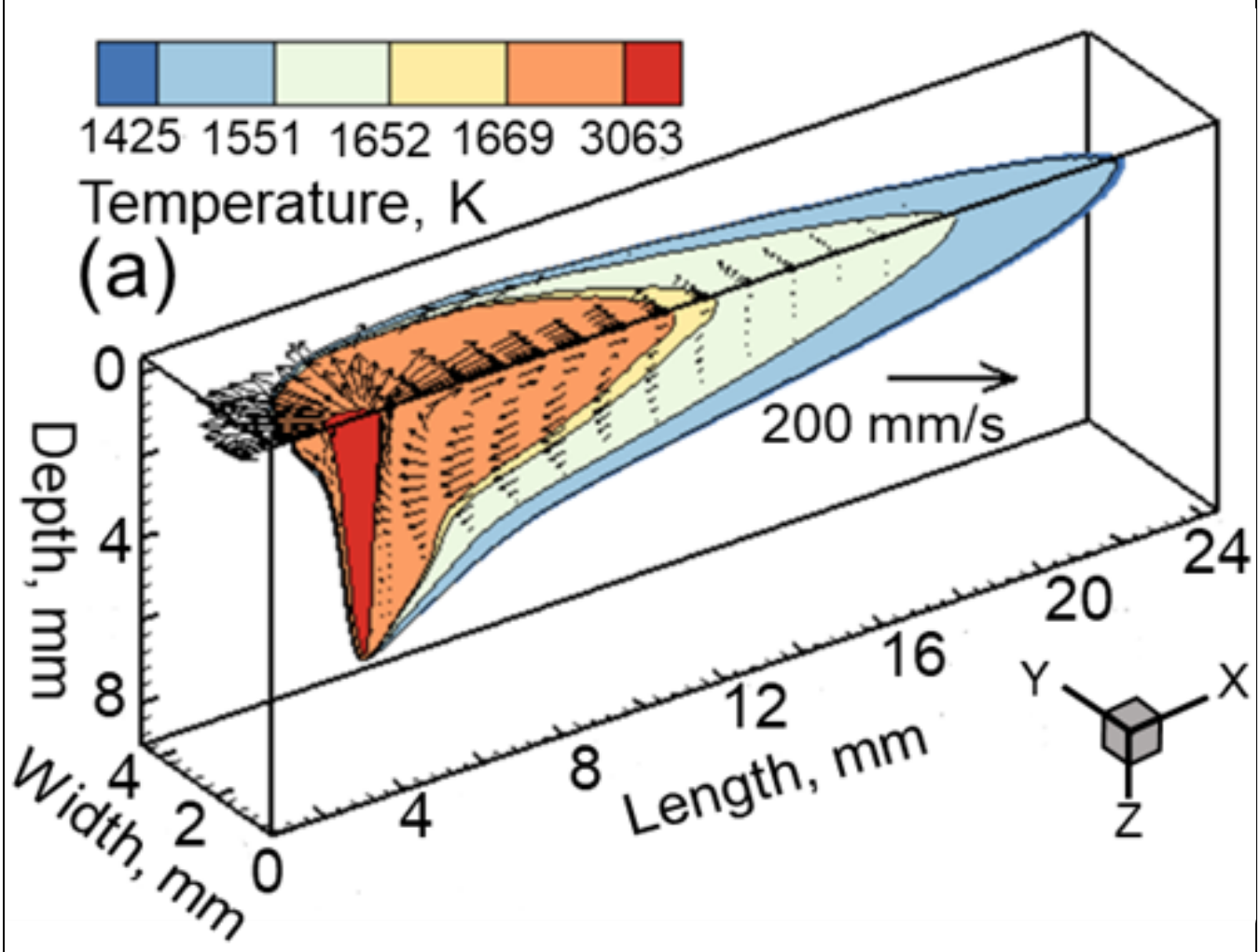

Figure 5. The calculated temperature and velocity fields during keyhole mode laser welding (without wobble) of IN 740H for 5 kW power and 12.7 mm/s welding speed. One-half of the pool is shown in a 3D isometric view due to symmetry across the vertical plane (XZ). The liquid metal flow is shown by the black velocity vectors and a reference vector is shown to estimate their magnitudes.

Clyne and Davies [1,2] proposed a hot cracking susceptibility coefficient, which is the ratio of the duration when the solid-liquid two-phase region is vulnerable to cracking and the relaxation time available for the stress relief process. The vulnerable time is defined in their model as the time needed for the solid-liquid mixture to solidify from the solid fraction of 0.9 to 0.99. During this period, the liquid metal available in the two-phase solid-liquid mixture is thought to be insufficient to compensate for the shrinkage of the last liquid. On the other hand, the relaxation time is defined by the progression of solidification during changes in the solid fraction from 0.4 to 0.9, where sufficient liquid is available to backfill the shrinkage. The procedure for the calculation of the hot cracking susceptibility coefficient is illustrated in Figure 6a. A high value of the coefficient indicates a greater time of exposure of the two-phase mixture to vulnerable conditions indicating a greater likelihood of cracking. As illustrated in Figure 6a, specific locations where

the solid fractions are 0.4, 0.9, and 0.99 within the two-phase region in the molten pool are needed to use the hot cracking model. They are calculated from the three-dimensional temperature field which depends on the welding variables such as laser power and welding speed. Furthermore, the cracking susceptibility coefficient can be calculated at different depths of welds. The relation between temperature and the solid fraction is obtained from the Scheil curve calculated from the thermodynamic package ThermoCalc. The calculations show that temperatures of 1425K, 1551K, 1652K, and 1669K corresponded to solid fractions of 0.99, 0.9, 0.4, and 0, respectively. The solid fractions contours at three depths are shown in Figure 6b, Figure 6c and Figure 6d. They show the green regions bound by solid fractions between 0.4 and 0.9, which represent the relaxation region, and the red regions bound by solid fractions of 0.9 and 0.99, which represent the vulnerable region at three depths.

Several XY horizontal cross-sections which represent various weld depths are considered to examine the changes in the lengths of vulnerable and relaxation regions and the corresponding hot cracking susceptibility coefficients. The weld pool and the mushy zone lengths decrease with increasing depth from the pool surface. The coefficients calculated for 5, 7.5, and 10 kW laser powers and 12.7 mm/s welding speed shows that for each power, the ratio of the vulnerable time to relaxation time increases continuously with depth as shown in Figure 7a. Furthermore, the depths corresponding to the vulnerable time to the relaxation time of 1.2 matches the depths where cracks are observed experimentally in each case (Table 1). Figure 7b shows a plot of the location of the cracks observed experimentally to the depth at which the ratio of the vulnerable time to relaxation time has a ratio of 1.2. The agreement shows that for the deep penetration keyhole mode laser welding of alloy 740H, the crack depth observed experimentally agrees with that calculated theoretically for a ratio of vulnerable time to relaxation time ratio of 1.2. When this threshold is crossed, i.e., when the value of the crack susceptibility coefficient is higher than 1.2, no other cracks have been observed experimentally.

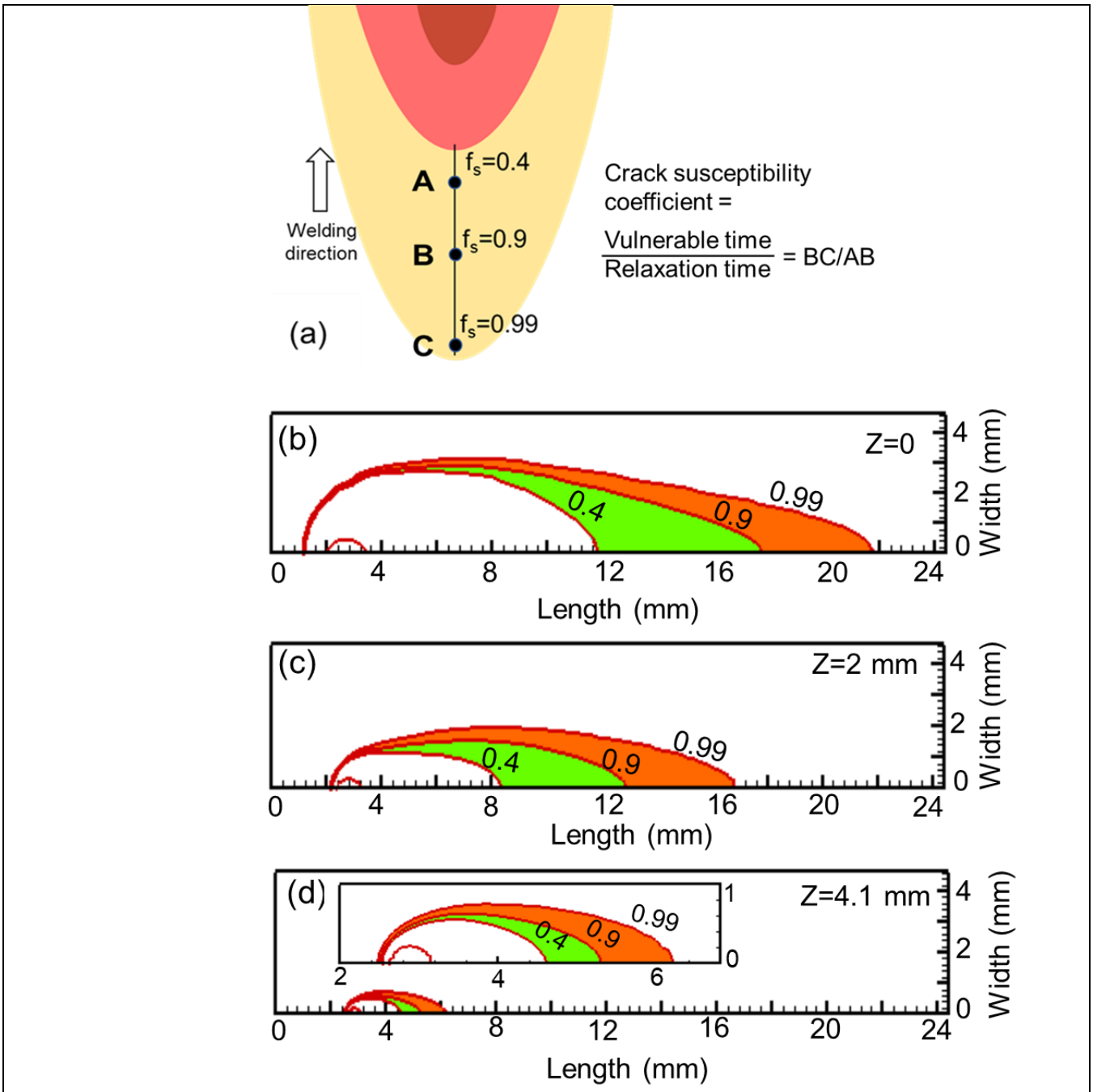

Figure 6. (a) A schematic diagram showing the location of different solid fractions (f_s) in the mushy zone. The contours for solid fractions of 0.4, 0.9, and 0.99 for horizontal cross-sections (XY planes) with 5 kW at Z=0 mm indicate contours at (b) the top surface, (c) the Z=2 mm plane, and (d) the Z=4.1 mm plane.

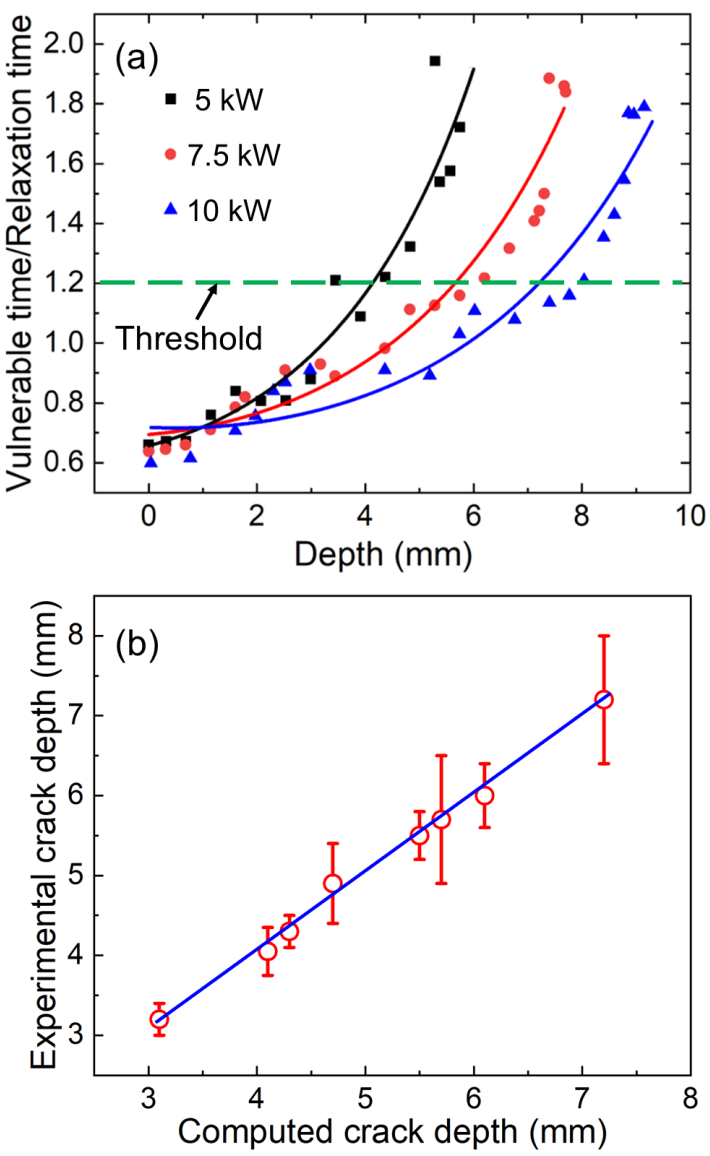

Figure 7. (a) The calculated ratio of vulnerable time to relaxation time (cracking susceptibility coefficient) for different laser powers and 12.7 mm/s welding speed; (b) Relation between computed and experimental crack depth for different welding variables (Table 1).

As seen in Figure 7a, the computed values of the crack susceptibility coefficient increase with depth. Why then no other cracks are observed at higher depths? It seems that once the value of the coefficient reaches 1.2, a higher value of the coefficient does not nucleate new cracks, but rather propagates the existing crack. This threshold value of the ratio holds for all powers and speeds investigated in this work and it allows identification of the depth where the cracks appear in each case for the welds without wobble. Increasing laser power (at constant welding speed) while providing greater depth of weld penetration also shifts the crack to greater depths (Figure 7a). *Model development of wobble welding are currently in progress to understand the absence of such cracks in wobble mode.*

Table 1. Comparison of experimentally observed crack depth and that predicted by using the model.

Laser Power (kW)	Welding speed mm/s	Crack depth (Experiment) mm	Crack depth from crack susceptibility coefficient of 1.2
5	12.7	3.7- 4.4	4.1
7.5	12.7	5 - 6.5	5.7
10	12.7	6.4 - 8	7.2
5	25.4	2.9-3.4	3.2
7.5	25.4	4.3 - 5.4	4.7
10	25.4	5.5-6.3	6.1
7.5	38.1	4 - 4.6	4.3
10	38.1	5.4 -5.9	5.5

References

[1] T. W. Clyne, G. J. Davies, British Foundryman 74 (1981) 65-73.
[2] T. W. Clyne, M. Wolf, W. Kurz, Metal. Trans. B 13 (1982) 259-266.

Update on Go/No Go Decision Pt #1: Performance of Deep Penetration Land Welds and HLAW filler weld material

Creep testing of Welds 2A, 2B, 4A, 4B, and 3A using the conditions in Table 2 has been completed. The resulting creep curves are plotted in Figure 8. The creep behavior of specimens containing conventional GTA welds under the same conditions are also plotted in Figure 8 using dashed lines. One notable observation includes the creep rates for the laser-only welded specimens - specimen 3A-1 in Figure 8a and 3A-2 in Figure 8b – were considerably faster than the HLAW specimens under the same conditions. This is likely due to differences in the width of the laser welds versus that of the HLAW and GTA welds. Laser welds are, by nature, very narrow and occupy only a small portion of the gage section of the creep specimen. However, the GTA and HLA welds occupy the greater portion of the gage section of the creep specimen and the macroscopic creep behavior of these specimens is closer to that of the weld. In the laser welded specimens, the macroscopic creep behavior has a larger contribution from the base metal (which is relatively fine versus weld metal and tends to creep faster). However, the creep rupture lifetime of laser welded and HLA welded specimens is comparable at both temperatures, indicating the weld is controlling the rupture lifetime.

The other notable observation is that the creep behavior of the laser welded specimens and the HLAW specimens is consistent with the GTAW specimens, possibly slightly better, i.e., slightly longer creep rupture lifetimes. In general, the creep behavior of HLAW specimens is more consistent than specimens with GTA welds, i.e., the dashed curves in Figure 8. Some variation in creep rupture lifetime of the HLAW is observed but appears to be consistent with the variation in creep lifetime observed in specimens with a GTA weld. HLAW specimens exhibiting a shorter creep rupture lifetime may be influenced by the small cracks in the weld shown in Figure 2. However, as a minimum, when the creep data from the laser welded specimens and the HLA welded specimens are placed in the stress-rupture

plot for 740H welds, Figure 9, they are consistent and, as a minimum, no worse than convention GTAW creep behavior.

Table 2. Summary of Welds and Test Conditions for Creep Testing

Plate Type	Plate ID	Weld ID	Specimen ID	Creep Testing Conditions	Creep Testing Location	Weld Conditions
Plate Type 1	2	A	**2A-1**	750°C, 350 MPa	PES	Campaign 2 – 25 ipm, 60° groove angle, infinity laser wobble, 3 kW, 4 mm amplitude, ~23.5 kJ/in (?)
	2	A	**2A-2**	800°C, 240 MPa	PES	
	2	B	**2B-1**	750°C, 350 MPa	PES	Campaign 2 – 25 ipm, 45° groove angle, infinity laser wobble, 3 kW, 4 mm amplitude, ~23.5 kJ/in(?)
	2	B	**2B-2**	800°C, 240 MPa	PES	
	4	A	**4A-1**	750°C, 350 MPa	PES	Campaign 3 – weld #Z10805, 20 ipm, 60° groove angle, Circular laser wobble, 2kW, 4 mm amplitude, ~19 kJ/in (?)
	4	A	**4A-2**	800°C, 240 MPa	PES	
	4	B	**4B-1**	750°C, 350 MPa	PES	Campaign 3 – Weld #Z10727, 20 ipm, 60° groove angle, Figure 8 laser wobble, 2 kW, 4 mm amplitude, ~19 kJ/in (?)
	4	B	**4B-2**	800°C, 240 MPa	PES	
	6	A	**6A-1****	750°C, 350 MPa	PES	Campaign 4 – weld# Z11112, TS=20 ipm, 60° groove angle, WFS = 7.5 m/min, 0.045" dia 740H wire, Star wobble, 51 Hz, 6 mm amplitude, 2 kW
	6	A	**6A-2****	800°C, 240 MPa	PES	
	6	A	**6A-3****	TBD (10,000 hr)	INL	
	6	A	**6A-4****	TBD (10,000 hr)	INL	
	6	B	**6B-1****	750°C, 350 MPa	PES	Campaign 4 – weld# Z11116, TS=20 ipm, 60° groove angle, WFS = 7.5 m/min, 0.045" dia 740H wire, Star wobble, 51 Hz, 6 mm amplitude, 3 kW
	6	B	**6B-2****	800°C, 240 MPa	PES	
	6	B	**6B-3****	TBD (10,000 hr)	INL	
	6	B	**6B-4****	TBD (10,000 hr)	INL	
Plate Type 2	3	A	**3A-1**	750°C, 350 MPa	PES	PSU – Laser weld (7.5 kW), no wobble, ~15 kJ/in
	3	A	**3A-2**	800°C, 240 MPa	PES	
	3	B	**3B-1***	750°C, 350 MPa	PES	
	3	B	**3B-2***	800°C, 240 MPa	PES	
	5	A	**5A-1***	750°C, 350 MPa	PES	
	5	A	**5A-2***	800°C, 240 MPa	PES	
	5	B	**5B-1***	750°C, 350 MPa	PES	
	5	B	**5B-2***	800°C, 240 MPa	PES	

*These will be sent at a later date
** Sent out for creep specimen fabrication

Since the creep data for these short-term tests on HLAW and laser-welded specimens are, at the very least, equivalent to the creep behavior of GTA welds in Alloy 740H, the criteria associated with the Go/No Go Decision Point #1has been satisfied, as outlined in the "Project Management Plan: Multi-pass Hybrid Laser Arc Welding of Alloy 740H, rev. 1", and the project has passed this decision point and may move on to the remaining tasks.

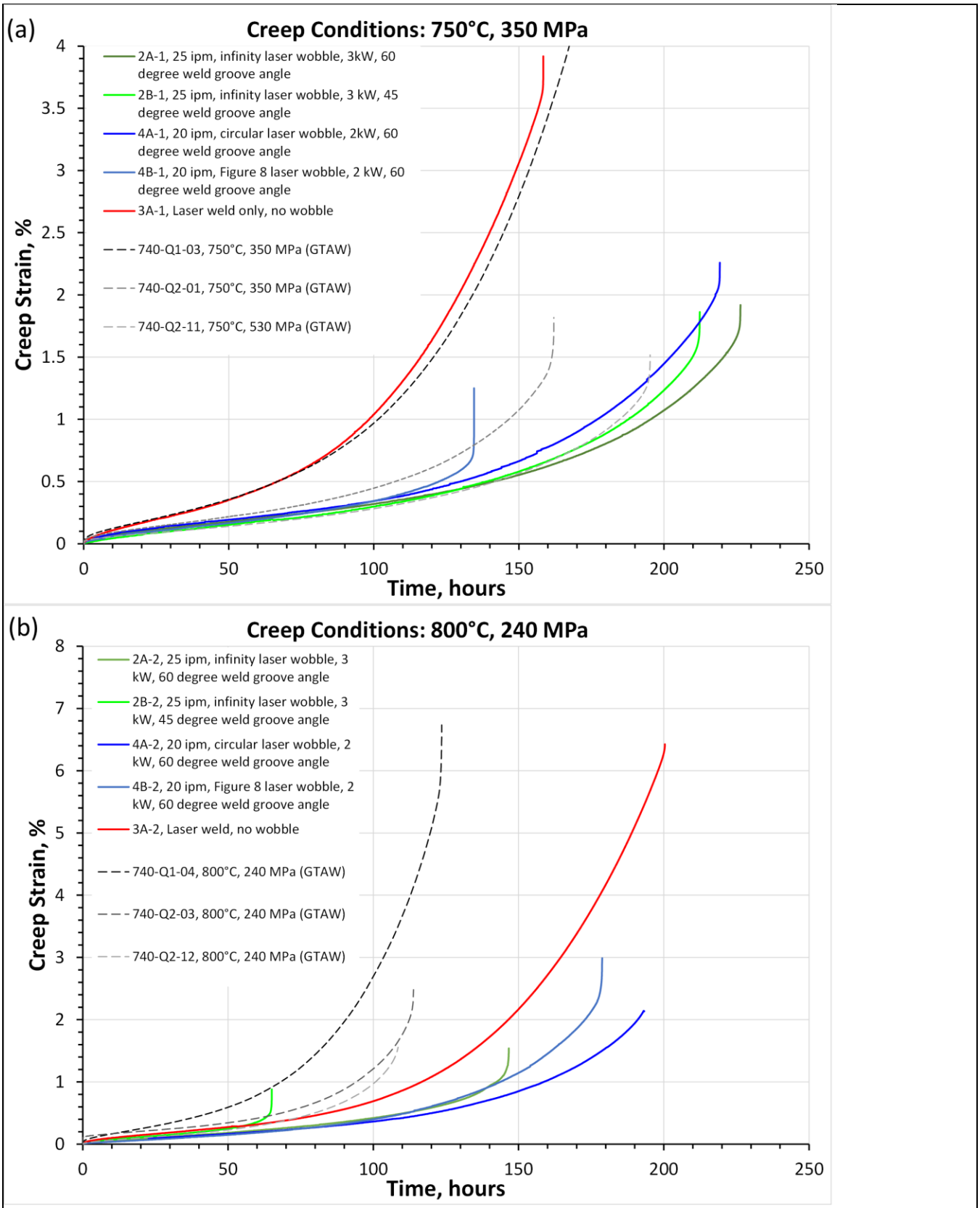

Figure 8. (a) Creep behavior at 750°C and 350 MPa and (b) 800°C, 200 MPa.

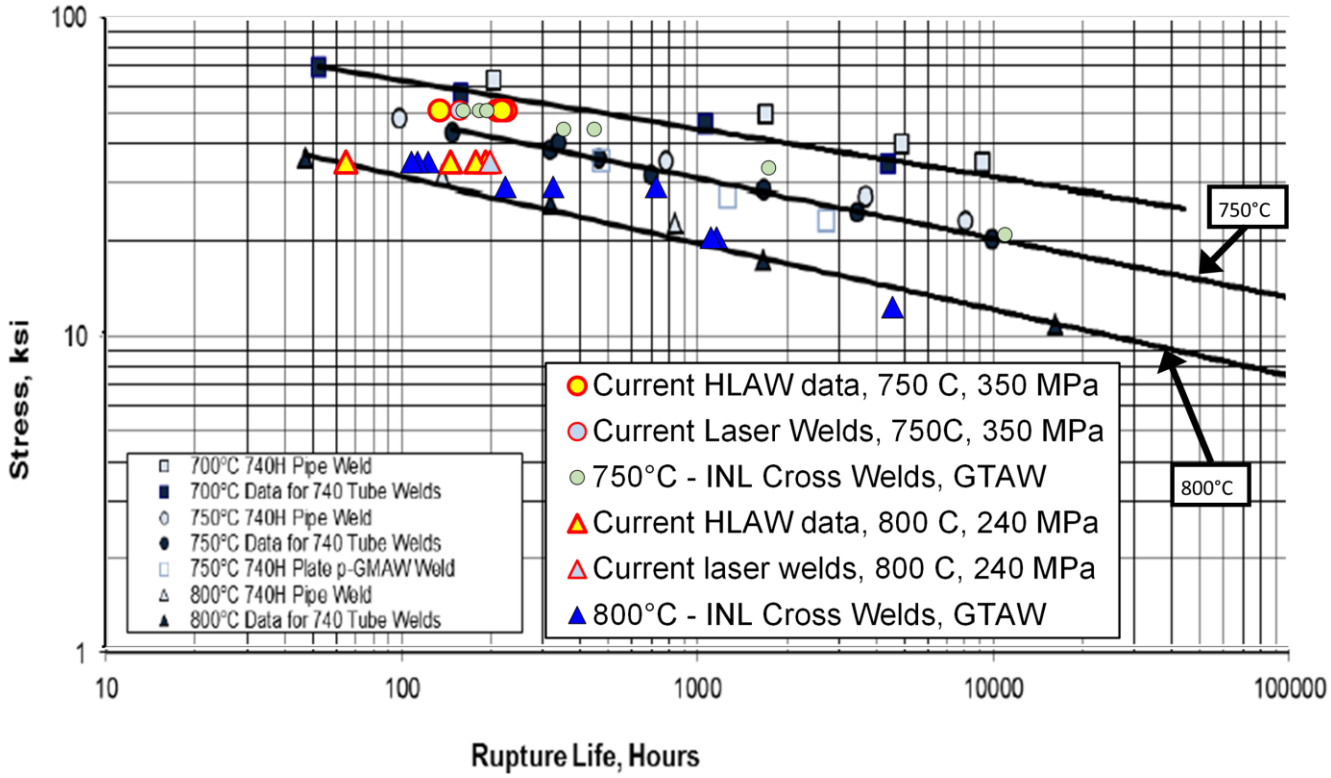

Figure 9. Stress rupture plot showing data from Special Metals Datasheet for Alloy 740H as well as GTAW data for 740H obtained from a previous project.

ISSUES

None identified at this time

Report Prepared By	Date
Thomas M. Lillo, INL; Todd Palmer, PSU	1/24/2022